LETTER

Instabilities and Pattern Transformation in Periodic, Porous Elastoplastic Solid Coatings

Srikanth Singamaneni,[†] Katia Bertoldi,[‡] Sehoon Chang,[†] Ji-Hyun Jang,[§] Edwin L. Thomas,*[,†] Mary C. Boyce,*[,‡] and Vladimir V. Tsukruk*[,†]

School of Materials Science and Engineering and School of Polymer, Textile, and Fiber Engineering, Georgia Institute of Technology, Atlanta, Georgia 30332-0245, and Department of Mechanical Engineering and Department of Materials Science and Engineering and Institute of Soldier Nanotechnologies, Massachusetts Institute of Technology, Cambridge, Massachusetts 02139-4307

ABSTRACT Pattern transformation in periodic microporous elastoplastic solid coatings is caused by a buckling of the struts and a rotation of the nodes under compressive stresses. The results of a nonlinear numerical investigation confirm the critical role of the bifurcation of the periodic solid under compressive stresses. In striking contrast to the earlier observations of elastic instabilities in porous elastomeric solids, the elastic−plastic nature of the cross-linked periodic microstructure studied here provides the ability to lock in the transformed pattern with complete relaxation of the internal stresses. The study unveils a novel deformation mode in porous periodic solids in the form of organized buckling instability of weak strut elements.

KEYWORDS: interference lithography structures • mechanical instabilities • pattern transformation • buckling behavior

Microscopic analogues of periodic cellular structures in which the periodicity and the pore size are in the submicron scale are important for a wide variety of applications ranging well beyond structural materials. Applications include photolithography, photonic and phononic band-gap materials, microfluidic networks, porous biomaterials as tissue engineering scaffolds, and DNA−protein microarrays (1−5). When subjected to external stresses caused by direct mechanical loading or internal stresses due to changes in the osmotic pressure, differential thermal expansion, or partial swelling, the periodic porous microstructure can become unstable at a certain critical point.

Buckling mechanical instabilities responsible for these dramatic transformations are ubiquitous phenomena observed at all length scales in a wide range of materials in both natural and man-made systems (6−16). Buckling instabilities have also been demonstrated to be instrumental in controlling adhesion, facilitating flexible electronics, fabricating microfluidic structures, providing means for micro- and nanopatterning, and designing optical microdevices (17−19). Reversible pattern transformation in periodic elastomeric structures at the millimeter scale subjected to a simple load has been uncovered (16, 20, 21). Even more recently, instability in the surface relief elastomeric structures was employed to pattern nanoparticles (22). These mechanical instabilities might lead to a dramatic transformation of the spatial organization, a phenomenon rarely addressed and discussed on a quantitative level.

Here we report on organized instability in microporous elastoplastic solids resulting in a dramatic transformation of the original periodic organization. This transformation is triggered by compressive stresses and resulted in the replacement of the initial square lattice of cylindrical pores with a peculiar pattern of alternating anisotropically collapsed pores.

The porous, periodic, solid polymer structure employed here has been fabricated with multiple-laser-beam interference lithography (IL) from a negative photoresist, epoxy derivative of a bisphenol A Novolac photocurable resin, SU8, which is widely utilized in photolithography technology (23−26). Periodic porous SU8 microframe structures with square lattice were fabricated using IL as described in detail elsewhere (see the Experimental Section) (27). Figure 1a schematically shows the unit cell and a 4 × 4 lattice of the pore arrays identifying the characteristic x_1, x_2, and x_3 directions. Figure 1b shows the atomic force microscopy (AFM) images of the pristine microframe with the corresponding FFT (as insets) reflecting the square array of cylindrical pores. The periodicity of the square lattice was 830 nm, the radius of the cylindrical pores was 190 nm, and the porosity was 20%. The thickness of the microframe structures was 3 μm, making the aspect ratio nearly 8. AFM nanomechanical measurements showed the average modulus of the SU8 structures as 1.3 GPa (28).

Initially, we verified that conventional filling (capillary infiltration) of the SU8 microframe porous structure with a rubbery phase [2% polybutadiene (PB)] from solution does not affect the initial structure: instead, finely separated PB microphases localized within the pores form a characteristic checkerboard pattern (see Figure S1 in the Supporting

* To whom correspondence should be addressed. E-mail: elt@mit.edu (E.L.T.), mcboyce@mit.edu (M.C.B.), vladimir@mse.gatech.edu (V.V.T.).
Received for review September 25, 2008 and accepted November 19, 2008
[†] Georgia Institute of Technology.
[‡] Department of Mechanical Engineering, Massachusetts Institute of Technology.
[§] Department of Materials Science and Engineering and Institute of Soldier Nanotechnologies, Massachusetts Institute of Technology.
DOI: 10.1021/am800078f

Published on Web 12/18/2008

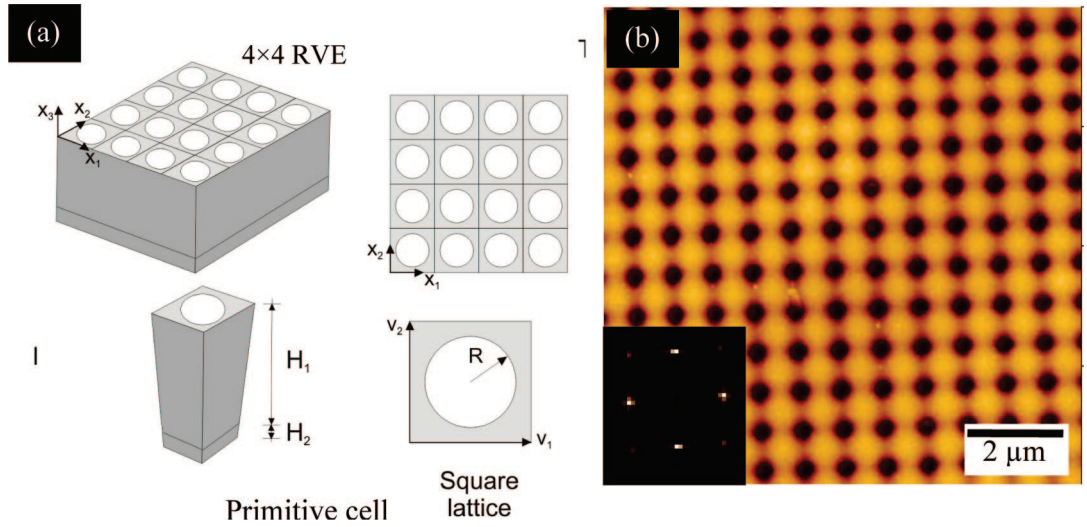

FIGURE 1. (a) 4 × 4 periodic representative volume elements (top row) and corresponding primitive cells (bottom row) for a square array. (b) AFM image of the pristine microframe structures with a square lattice. (Inset shows the FFT of the AFM image.)

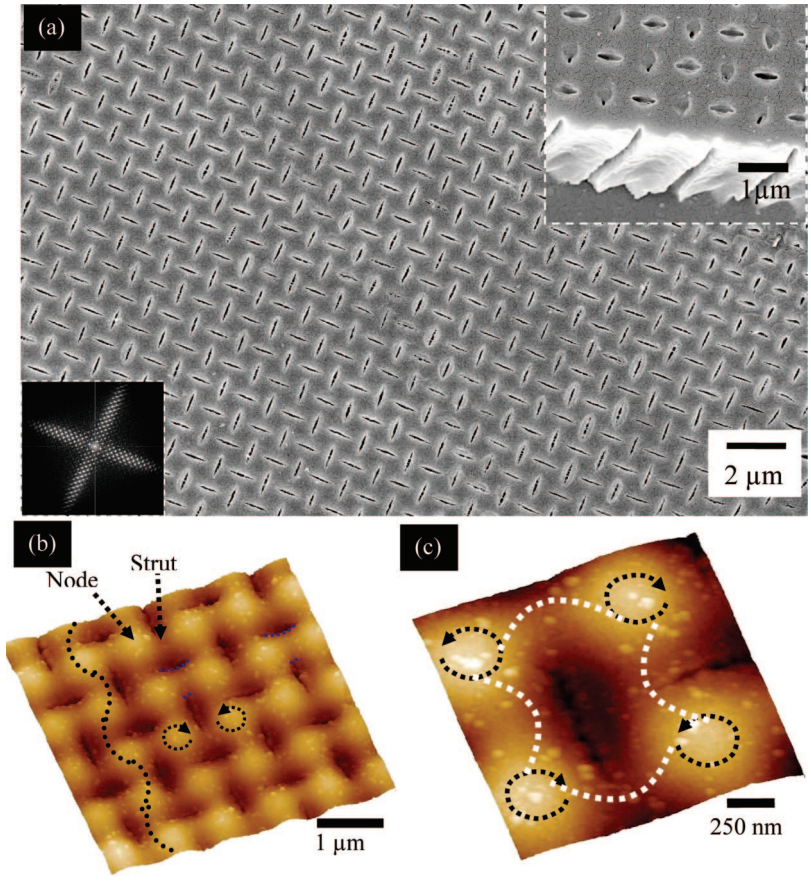

FIGURE 2. SEM images of transformed patterns of a square lattice showing large-scale uniformity. Inset in the bottom: FFT of the transformed patterns. Inset in the top: SEM image depicting the through elliptical pores along the total thickness of the SU8 microframe. (b) AFM topographical image of the transformed pattern showing the deformation modes of the struts (bending) and the nodes (rotation) of a square lattice. (c) High-magnification AFM image showing rotation of the nodes, resulting in the bending of the struts.

Information) (28). In sharp contrast, in situ solution photopolymerization of an acrylic acid monomer performed directly in the cylindrical pores (see experimental details and Figure S2 in the Supporting Information) resulted in a fundamental transformation of the initial porous structure. The initial square array of cylindrical micropores has been transformed into periodic, mutually orthogonal, highly collapsed elliptical pores. A dramatically different lattice with a perfectly regular, nontrivial geometry of alternating anisotropic slitlike pores expands across the macroscopic area (Figure 2a). Interestingly, the original periodicity of the micropore lattice remains constant (within 1%) despite the global shape transformation. Transformed regions are extremely uniform extending to surface areas up to a fraction of a millimeter. We have also investigated the pattern transformation in a hexagonal lattice structure. The oblique

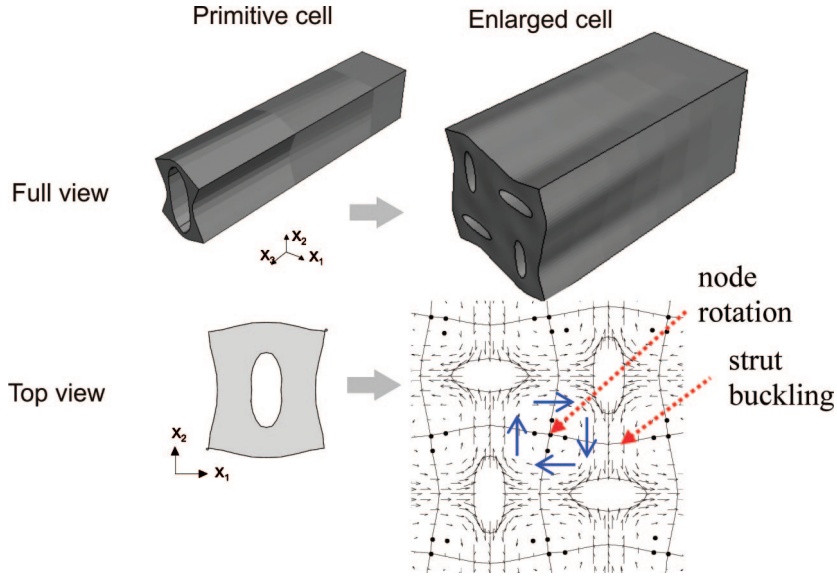

FIGURE 3. Eigenmode of the microscopic instability for the infinite square array of circular holes as predicted by the Bloch wave analysis and the top view of the strain field with arrows showing the direction of local displacements.

lattice has been transformed into an array of sheared pores with the shear direction alternating back and forth from row to row, resembling a common herringbone pattern as will be discussed in detail elsewhere (see Figure S3 in the Supporting Information).

AFM shows fine details of the transformed pattern morphology (Figure 2b). The pattern of alternating elliptical micropores is identical along the x_1 and x_2 directions, with the characteristic, double-bump shape reflecting the alternating depth of the AFM tip penetration along short and long axes of the collapsed pores (Figures 2b and S4 in the Supporting Information). The AFM image of Figure 2b shows the nodes (elevated round areas) and struts (ridges connecting nodes) of the square lattice microframe structure. At a microscopic level, the pattern transformation can be related to bending of the struts in alternating directions (along x_1 and x_2) and the rotation of the nodes in clockwise and anticlockwise directions (20) as indicated on the AFM image (Figure 2c), with the resulting instabilities frozen after transformation. Despite the fact that the substrate strongly constrains the deformation of the porous structure, the deformation pattern propagates through the whole thickness of the film (inset of Figure 2a).

We suggest that the high compressive stresses originate from the slow evaporation of water from inside the micropores, causing the swollen poly(acrylic acid) (PAA) network grafted to the pore walls to shrink significantly (4-fold). For further insight into the mechanistic aspect of the pattern transformation observed here, numerical investigations of the behavior of the periodic microporous solids were conducted utilizing the nonlinear finite-element approach with eigenvalue analysis successfully applied earlier to elastomeric porous solids (see experimental section) (16, 20). The bifurcation modes of the infinite periodic porous solid are investigated by conducting a Bloch wave analysis on the primitive cell with parameters taken from independent experimental measurements (Figure 1a and see the Supporting Information) (29).

Our bifurcation analysis demonstrates that during the initial deformation the square array of cylindrical pores undergoes a transformation at a critical engineering strain of −0.013 (applied stress of 60 MPa). This symmetry change results in a 4 times enlarged representative cell now consisting of two primitive cells in both lattice directions (Figure 3). The displacement field calculated for such a compression confirms the rotation of the nodes and the resulting buckling of the struts, as was suggested from AFM images (Figure 2b).

To capture the post-transformation behavior, an imperfection in the form of the most critical eigenmode was introduced into the mesh. The plot of Figure 4a depicts the stress−strain behavior for both cases of the bottom surface fixed only in the x_3 direction (denoted as "x_3 fixed") and in all three directions (denoted as "All fixed"). Images of the deformed configurations for the square array of cylindrical pores at different deformation regimes are shown in Figure 4b. As this simulation reveals, during the deformation, the cylindrical pores undergo gradual and homogeneous compression at very low strain below −0.01. This affinelike deformation is replaced by a cell bifurcation, leading to a sudden lattice transformation to a pattern of alternating, mutually orthogonal ellipses identical with those observed experimentally (Figures 2 and 4b). Once formed, the new pattern (point B, Figure 4) becomes further accentuated in shape such that the major axis of each ellipse lengthens while its minor axis shortens with increasing compressive strain (point C, Figure 4). The simulation suggests that the transformed pattern is composed of mutually orthogonal ellipses, resulting in both rotation of the nodes of the lattice and buckling of the struts, as suggested above (see Figure 3a for displacement flow distribution). Moreover, in contrast to the periodic elastomeric structures reported earlier, the dual (elastic−plastic) nature of the SU8 material deformation locks in the mechanical instabilities after the release of the

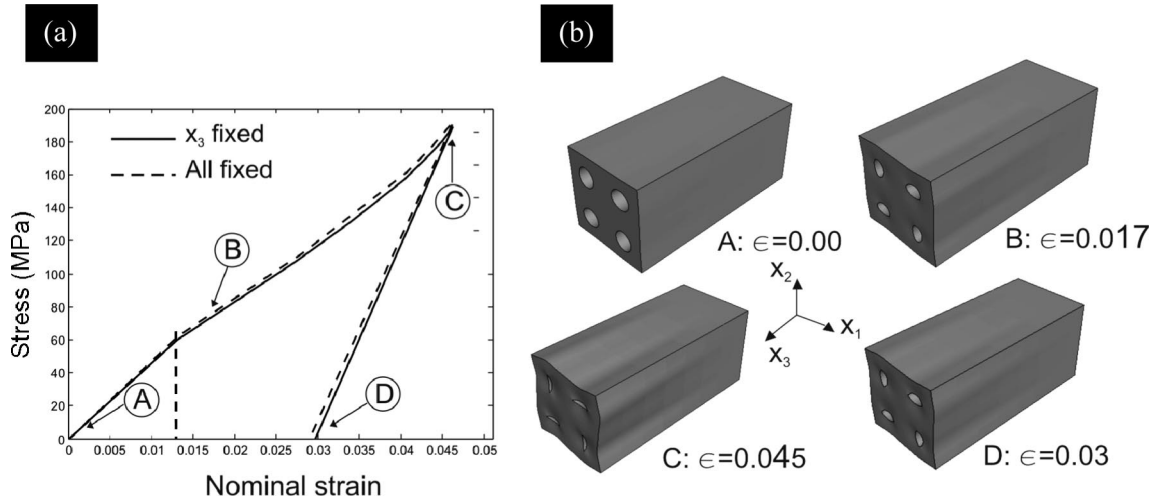

FIGURE 4. (a) Nominal compressive stress vs nominal strain curve calculated for the square array of cylindrical pores (the vertical dashed line shows theoretical critical strain). (b) Corresponding 3D images of the square lattice at different levels of macroscopic strain.

external stress, with internal stresses dissipated to a great extent (point D, Figure 4).

We estimated the ability of a shrinking PAA network confined within cylindrical pores to create a pressure on their inner sidewalls to trigger the instability event. The elastic modulus of PAA (polymerized under identical conditions) in a dry state was measured to be 54 MPa from AFM nanomechanical probing (see Figure S5 in the Supporting Information). Upon evaporation of 73% of the solvent, the PAA network shrinks by the same amount, exerting a retracting force on the sidewalls of the cylindrical pores. A strain of 0.54 in the PAA network asserts about 30 MPa stress on the solid structure, which is close to the transformation point B on the simulated stress−strain curve (Figure 4). The capillary forces during the evaporation of water in the pores also can, in principle, induce internal stresses. The capillary force can be estimated using the Laplace equation ($P = 2\gamma/r$) as 0.7 MPa, which is well below the critical stress required to cause mechanical instabilities in the microframe structure.

The pattern transformation observed here for elastoplastic microporous solids below the nominal glass transition temperature is different from the earlier observation of similar phenomena in elastomeric porous solids in several ways. First, the pattern transformation has been achieved at a significantly smaller spatial scale (submicron) and strain level (below −1%) compared to the earlier reports. The lower critical strain is due to the lower elastic limit (2−3%) in which an affine deformation can be accommodated in a cross-linked SU8 material below the glass transition temperature compared to the elastomers (100−200%) employed in earlier reports. Second, previous pattern transformations were observed in periodic elastomeric solids, so that upon removal of the state of stress the transient pattern transformed back to the initial state. Here, instead, the pattern transformation has been observed in a cross-linked elastoplastic porous polymer, which facilitates the retention of the frozen instabilities and corresponding transformed periodic pattern and its preservation even after prolonged thermal annealing at temperatures close to 120 °C (about the glass transition temperature).

The earlier reports predicted or demonstrated the pattern transformation in periodic porous materials due to external uniaxial or biaxial compression; instead, here we have observed and analyzed the pattern transformation initiated by the compressive stresses generated inside the cylindrical pores by rubbery materials grafted to the walls in the course of its polymerization and solvent evaporation. We believe that the mechanism of transformation of organized microporous solids via localized bifurcation of the primitive cell with rotation of nodes combined with the bending or buckling of struts can be important in the range of complex physical phenomena critical for diverse fields such as tunable photonic crystals, porous scaffolds for tissue engineering, structures with tunable transport properties, or porous-shape memory alloys in metallic and polymeric stents (30, 31).

EXPERIMENTAL SECTION

Fabrication of SU8 Microframes. 2D square and hexagonal patterns were fabricated using multibeam IL according to the usual procedure (27). The fabrication involved a two-step sequential, double exposure with a 90° rotation of the sample to the interference pattern of two equal-intensity laser beams for the square lattice. The transfer of the light intensity pattern into an SU8 photoresist platform via laser-initiated cationic polymerization results in each 2D-patterned structure. The Gaussian output from the laser was cleaned up and expanded using a spatial filter and recollimation setup.

The materials platform consisted of Epon-SU8 (Miller Stephensen) as a photoresist (a multifunctional epoxy derivative of a bisphenol A Novolac), H-Nu 470 (Spectra group) as a photosensitizer that absorbs the visible light and electron transfers to an onium salt, [(octoxyphenyl)phenyl]iodonium hexafluoroantimonate (UCB Radcure) as a photoacid generator, and trioctylamine to compensate for the nonzero background arising from the interference intensity. The glass substrate was treated with a thin (700 nm) buffer layer of pre-cross-linked SU8 material to ensure attachment of the structured polymer film to the substrate via chemical grafting. A 3-μm-thick SU-8 film was subsequently spin-coated on top of the existing cross-linked SU-8 film at a spin speed of 2000

rpm. The IL exposure was done using a 532-nm continuous-wave Nd:YAG laser with an intensity of 1.5 W for 8−15 s to give a total exposure dose of 12−22 J/cm^2. After the 3-μm-thick film is baked at 75 °C for 3 min, the resultant cationic photopolymerization only takes place in regions that were exposed to high intensities of light. The uncured regions are developed away in propylene glycol monomethylether acetate, followed by rinsing with isopropyl alcohol. No further heat treatment is applied. The glass transition temperature of the SU8 cured under similar conditions (including the 5-min UV exposure to acrylic acid) was found to be 120 °C from the DMA measurements.

In Situ Polymerization of Acrylic Acid in Submicron Pores. To fabricate filled microframes (Figure S2 in the Supporting Information), pristine microframes were treated with ethanolamine to reduce the hydrophobicity and induce surface hydroxyl groups (32). Following the ethanolamine treatment (which resulted in a decrease in the contact angle from 90° to 30°), the sample was thoroughly washed in nanopure water and placed in a vial containing 1% acryloyl chloride in ethyl ether for 90 min. AFM imaging at this stage in various locations of the sample revealed no signs of a transformed pattern. Then, the sample was washed thoroughly and immersed in a 20% acrylic acid solution with a 5% UV initiator and a 2% UV cross-linker (acrylamide), allowing the acrylic acid solution to infiltrate the pores. Finally, the sample was exposed to UV light (365 nm, 20 mW/cm^2) to initiate the polymerization of acrylic acid. The pH of the monomer with the initiator and cross-linker was 2.3, keeping the carboxylic moieties on PAA in the neutral state. The cross-linked PAA materials filling the micropores are in a swollen state in water (73% water).

Nanomechanical Measurements. AFM nanomechanical measurements have been conducted to address the spatial distribution of stiffness and the elastic response in the 2D microframe structures in accordance with the procedure adapted in our laboratories (33−35). Nanomechanical measurements are conducted in the elastic regime, with a small indentation depth allowing elastic recovery of the surface areas as presented in our recent paper (27). Representative force−volume data for the PAA phase are presented in Figure S4 in the Supporting Information.

Numerical Simulations. Numerical simulations were conducted within the nonlinear code ABAQUS/Standard, version 6.6-1. Each mesh was constructed of 15-node, quadratic, hybrid, 3D elements (ABAQUS element type C3D15H). In the numerical analyses, an infinite array of circular holes has been considered in the x_1-x_2 plane parallel to the holes, so that the analyses could be conducted both on the primitive cell and on the multicell representative volume elements (RVEs; Figure 1a). To respect the periodicity of the structure, a series of constraint equations were applied to the surfaces of the primitive cell (not on the top and bottom surfaces), providing general periodic boundary conditions (36). The top surface is traction-free, while in order to account for the effects of possible different boundary conditions, two different constraint conditions have been considered for the bottom surface: the bottom surface is fixed only in the x_3 direction, and the bottom surface is fixed in all directions. Because the periodicity of the structure is limited to the x_1-x_2 plane, here the Bloch wave vector $\mathbf{k}_0$ has no component in the x_3 direction ($k_{03} = 0$).

The square array is composed of cylindrical pores with a radius $R = 190$ nm and a primitive cell Y defined by the lattice vectors $\mathbf{v}_1 = [830\ 0]$ nm and $\mathbf{v}_2 = [0\ 830]$ nm (Figure 1a). The pores are considered to be 3 μm long in the x_3 direction, and the porous structures are bonded to a substrate that is 700 nm thick. The stress−strain behavior of the photo-cross-linked epoxy SU8 material is captured using a rate-independent elastoplastic model because the small rate dependency does not influence the pattern transformation. The initial Young's modulus was taken to be 1.3 GPa, and Poisson's ratio is taken to be 0.33. The other material parameters are derived from values recently measured, taking them to linearly scale with the initial Young's modulus. A Mises yield surface and isotropic hardening are used with a yield stress of 60 MPa and a strain hardening modulus of 300 MPa. In correspondence with the periodicity of the transformed patterns, RVEs consisting of 2×2 primitive cells are considered to simulate the stress−strain response of the square array.

Acknowledgment. The work presented here is supported by NSF Grant CMS-0709586 and the Institute for Soldier Nanotechnologies of the U.S. Army Research Office (under Contract DAAD-19-02-0002). The authors thank Dr. Sergiy Peleshanko and Whitney Davis for technical assistance.

Supporting Information Available: Images of the pristine and transformed structures. This material is available free of charge via the Internet at http://pubs.acs.org.

REFERENCES AND NOTES

(1) Campbell, M.; Sharp, D. N.; Harrison, M. T.; Denning, R. G.; Turberfield, A. J. *Nature* **2000**, *404*, 53.
(2) John, S. *Phys. Rev. Lett.* **1987**, *58*, 2486.
(3) Ulbricht, M. *Polymer* **2006**, *47*, 2217.
(4) Théry, M.; Racine, V.; Pépin, A.; Piel, M.; Chen, Y.; Sibarita, J.-B.; Bornens, M. *Nat. Cell Biol.* **2005**, *7*, 947.
(5) Hollister, S. *Nat. Mater.* **2005**, *4*, 518.
(6) Bowden, N.; Brittain, S.; Evans, A. G.; Hutchinson, J. W.; Whitesides, G. M. *Nature* **1998**, *393*, 146.
(7) Efimenko, K.; Rackaitis, M.; Manias, E.; Vaziri, A.; Mahadevan, L.; Genzer, J. *Nat. Mater.* **2005**, *4*, 293.
(8) Mahadevan, L.; Rica, S. *Science* **2005**, *307*, 1740.
(9) Hiller, J.; Mendelsohn, J. D.; Rubner, M. F. *Nat. Mater.* **2002**, *1*, 59.
(10) Stafford, C. M.; Harrison, C.; Beers, K. L.; Karim, A.; Amis, E. J.; Vanlandingham, M. R.; Kim, H.-C.; Volksen, W.; Miller, R. D.; Simonyi, E. E. *Nat. Mater.* **2004**, *3*, 545.
(11) Jiang, C.; Singamaneni, S.; Merrick, E.; Tsukruk, V. V. *Nano Lett.* **2006**, *6*, 2254.
(12) Sun, Y.; Chi, W. M.; Jiang, H.; Huang, Y. Y.; Rogers, J. A. *Nat. Nanotechnol.* **2006**, *1*, 201.
(13) Gunawidjaja, R.; Ko, H.; Jiang, C.; Tsukruk, V. V. *Chem. Mater.* **2007**, *19*, 2007.
(14) Khang, D.-Y.; Xiao, J.; Kocabas, C.; MacLaren, S.; Banks, T.; Jiang, H.; Huang, Y. Y.; Rogers, J. A. *Nano Lett.* **2008**, *8*, 124.
(15) Huang, J.; Juszkiewicz, M.; de Jeu, W. H.; Cerda, E.; Emrick, T.; Menon, N.; Russell, T. P. *Science* **2007**, *317*, 650.
(16) Bertoldi, K.; Boyce, M. C.; Deschanel, S.; Prange, S. M.; Mullin, T. *J. Mech. Phys. Solid.* **2008**, *56*, 2642.
(17) Chan, E. P.; Smith, E. J.; Hayward, R. C.; Crosby, A. J. *Adv. Mater.* **2008**, *20*, 711.
(18) Sun, Y.; Rogers, J. A. *J. Mater. Chem.* **2007**, *17*, 832.
(19) Yoo, P. J.; Suh, K. Y.; Park, S. Y.; Lee, H. H. *Adv. Mater.* **2002**, *14*, 1383.
(20) Mullin, T.; Deschanel, S.; Bertoldi, K.; Boyce, M. *Phys. Rev. Lett.* **2007**, *99*, 084301.
(21) Bertoldi, K.; Boyce, M. C. *Phys. Rev. B* **2008**, *77*, 052105.
(22) Zhang, Y.; Matsumoto, E. A.; Peter, A.; Lin, P.-C.; Kamien, R. D.; Yang, S. *Nano Lett.* **2008**, *8*, 1192.
(23) Jang, J.-H.; Ullal, C. K.; Maldovan, M.; Gorishnyy, T.; Kooi, S.; Koh, C.; Thomas, E. L. *Adv. Funct. Mater.* **2007**, *17*, 3027.
(24) Moon, J. H.; Ford, J.; Yang, S. *Polym. Adv. Technol.* **2006**, *17*, 83.
(25) Maldovan, M.; Ullal, C. K.; Carter, W. C.; Thomas, E. L. *Nat. Mater.* **2003**, *2*, 664.
(26) Ullal, C. K.; Maldovan, M.; Thomas, E. L.; Chen, G.; Han, Y.-J.; Yang, S. *Appl. Phys. Lett.* **2004**, *84*, 5434.
(27) Choi, T.; Jang, J.-H.; Ullal, C. K.; Lemieux, M. C.; Tsukruk, V. V.; Thomas, E. L. *Adv. Funct. Mater.* **2006**, *16*, 1324.
(28) Singamaneni, S.; Chang, S.; Jang, J.-H.; Davis, W.; Thomas, E. L.; Tsukruk, V. V. *Phys. Chem. Chem. Phys.* **2008**, *10*, 4093.

(29) Triantafyllidis, N.; Nestorovic, M. D.; Schraad, M. W. *Jnt. Appl. Mech.* **2006**, *73*, 505.
(30) Xie, J.; Ihara, M.; Jung, Y.; Kwon, K.; Kim, S. H.; Kim, Y. H.; Matsuda, T. *Tissue Eng.* **2006**, *12*, 449.
(31) Zhao, Y.; Taya, M.; Kang, Y.; Kawasaki, A. *Acta Mater.* **2005**, *53*, 337.
(32) Nordström, M.; Marie, R.; Calleja, M.; Boisen, A. *J. Micromech. Microeng.* **2004**, *14*, 1614.
(33) Tsukruk, V. V.; Huang, Z.; Chizhik, S. A.; Gorbunov, V. V. *J. Mater. Sci.* **1998**, *33*, 4905.
(34) Shulha, H.; Kovalev, A.; Myshkin, N.; Tsukruk, V. V. *Eur. Polym. J.* **2004**, *40*, 949.
(35) Tsukruk, V. V.; Huang, Z. *Polymer* **2000**, *41*, 5541.
(36) Danielsson, M.; Parks, D. M.; Boyce, M. C. *J. Mech. Phys. Solids* **2002**, *50*, 351.

AM800078F